IEEE Access
Multidisciplinary | Rapid Review | Open Access Journal

Received May 18, 2020, accepted June 8, 2020, date of publication June 26, 2020, date of current version July 8, 2020.

Digital Object Identifier 10.1109/ACCESS.2020.3005237

Cross-Layer Design and Analysis of Wireless Geophone Networks Utilizing TV White Space

NAVEED IQBAL[1], SUHAIL AL-DHARRAB[1], (Senior Member, IEEE), ALI H. MUQAIBEL[1], (Senior Member, IEEE), WESSAM MESBAH[1], (Senior Member, IEEE), AND GORDON L. STÜBER[2], (Fellow, IEEE)

[1]Center for Energy and Geo Processing, Electrical Engineering Department, King Fahd University of Petroleum and Minerals, Dhahran 31261, Saudi Arabia
[2]School of Electrical and Computer Engineering, Georgia Institute of Technology, Atlanta, GA 30332, USA

Corresponding author: Naveed Iqbal (naveediqbal@kfupm.edu.sa)

This work was supported by the Center for Energy and Geo-Processing (CeGP), King Fahd University of Petroleum and Minerals (KFUPM), Dhahran, Saudi Arabia, under Grant GTEC1601.

ABSTRACT Traditional seismic data acquisition systems used for surveying during the exploration of oil and gas rely on cables between geophones and the data collection center. Despite the fact that cable-based systems provide reliable seismic data transfer, their deployment and maintenance costs increase substantially as the survey area increases in scale. Therefore, a three layer wireless network architecture is proposed in this work, which consists of wireless geophones (WG) and a data center with an intermediate wireless gateway node (WGN). This paper investigates the aggregate data throughput, transmission time, and energy consumption from WGs to the WGN in a wireless geophone network architecture based on the IEEE 802.11af standard. This standard is considered in order to have the maximum possible range and low power consumption due to operating in TV bands. Analytical expressions of the aforementioned quantities are derived using Markov chain models. Two Markov models are considered for this purpose: one for modeling the access method that allows multiple WGs to connect to a WGN and the other for representing a buffer in a WG. Since seismic data is recorded at regular intervals, arrivals of data packets in the buffer of the WG is deterministic. On the other hand, departure is random due to the multiple access method. Hence, in this work D/M/1/B queue is used for the first time to model the buffer in a wireless geophone. Furthermore, the physical layer constraints are also taken into account together with proper wireless path-loss channel models. The results obtained are useful for designing such wireless seismic networks without extensive simulations. In particular, the proposed joint medium access control, physical layer, and D/M/1/B model enables us to optimize the required number of WGNs. Finally, sectoring is also introduced in order to minimize the total number of WGNs needed to cover the whole surveying area.

INDEX TERMS Medium access layer, physical layer, queueing, sectoring, wireless geophones, D/M/1/B queue.

I. INTRODUCTION

For many years, oil and gas companies relied on cable-based architectures to transmit data from geophones to a data collection center. In land seismic surveys, cables are responsible for nearly 50% of total cost and 75% of total equipment weight [2]. Typically, data are collected by a large number of geophones deployed over an area of more than 20 km^2 [3]. Recently, there has been a growing interest to deploy wireless geophone networks for seismic acquisition especially in large land surveys [2]–[8]. In [2], future potential of wireless geophone structure is discussed for high-density land seismic acquisition. In [4], a nodal system is proposed where geophones store the seismic data and then the crew collects the stored data from the field. The design requirements of a wireless geophone network are discussed in [5], where multiband orthogonal frequency division multiplexing (MB-OFDM) is adopted for radio transmission. A hybrid approach of the wired and wireless network is proposed in [6]. To date, suggested technologies are not utilizing the full potential of the wireless communication network that is capable of competing with cabled systems [5]. Due to

The associate editor coordinating the review of this manuscript and approving it for publication was Wen Chen.

This work is licensed under a Creative Commons Attribution 4.0 License. For more information, see https://creativecommons.org/licenses/by/4.0/

power limitations, short-range and long-range transmissions are required to eliminate the cables. In short-range, wireless geophones (WG) send the recorded data to the wireless gateway node (WGN). The WGN then forwards all the received data to a storage and processing unit (recording cabin) in a long-range transmission.

For the design of wireless seismic acquisition system, it is necessary to understand the seismic data acquisition process. It consists of three main phases: shooting phase (source generates seismic waves), recording phase (geophones detect reflected waves from subsurface layers), and data delivery phase (synchronization, digitalization and forwarding). These phases are repeated at regular time intervals. In order to design a wireless geophone network for seismic acquisition, constraints such as transmission time, power limitation, and maximum attainable aggregate throughput need to be investigated keeping in view the fixed topology. Furthermore, the impairments introduced by the medium access control (MAC) and the physical (PHY) layers are very important, and hence, investigating the MAC and PHY layers for realistic conditions is essential for performance analysis. The analysis of throughput, transmission time, and power by considering MAC and PHY layers parameters is lacked in the aforementioned references. In this work, carrier sense multiple access method with collision avoidance (CSMA/CA) is considered for the communication between the WG and WGN. This medium access method is commonly used in such kind of networks, e.g., IEEE 802.11 and 802.15.4 standards.

There are three ways to test a network or a system; physical model (real test bed), a simulation model or a mathematical model. Mathematical/analytical models strive to reproduce the technical aspects and mechanisms that are widely seen in the standards (such as, IEEE 802.11 or 802.15.4) in order to track the performance of a network. In this work, a mathematical model is adopted for the first time to test the wireless system performance that is proposed for the seismic field survey. The reason is to enable seismologists to design the wireless seismic network based on their requirements without using less familiar softwares.

Since the PHY and MAC layers contribute to the major performance degradation in the network, these layers are considered to be the most effective layers in the protocol stack. Therefore, this paper focuses on the analysis of these layers. In the literature, there are numerous mathematical models to investigate the MAC behavior and test its performance and functionality. These models can be broadly classified into saturated [9], [10] and unsaturated traffic models [11]. In saturated traffic, a node or a WG (in our case) always has a packet ready for transmission, i.e., the buffer in a node never gets empty. However, in a real situation, a node possibly becomes idle when there is no packet in the buffer to transmit, this is known as an unsaturated condition. The situation of seismic acquisition network is similar to unsaturated traffic condition, since after sending a packet to the centralized entity (WGN in our case), the WG can enter an idle state.

The aim of this work is to model the communication process between WG and WGN using Markov chains. A well-known MAC layer model in the literature is Bianchi's Markov chain model for IEEE 802.11 [10]. This model mimics the MAC layer functionalities while considering ideal channel conditions with saturated traffic. This model finds a basis for many analytical studies [12]–[19]. Bianchi's model has been extended to analyze the delay [12], [13], packet reception rate [20], throughput [16] and MAC layer service time [14], [15] of the IEEE 802.11. Bianchi's model also provides foundation for the IEEE 802.15.4 model [9], [21]. However, simulation results show weak matching with the analytical results under unsaturated traffic [11]. In [18], Daneshgaran *et al.* develop a generalized MAC layer model for unsaturated traffic and combine it with the generalized PHY layer model for Rayleigh channels to be used for IEEE 802.11.

In this work, the proposed joint PHY, MAC and buffering model is built on the work of Daneshgaran *et al.* [18]. We extend this model so that it not only incorporates the general mechanisms at MAC and PHY layer, but also other PHY layer parameters and constraints, such as, Signal-to-Noise Ratio (SNR), encoding, modulation, and hardware and MAC layer functionality, i.e., request to send and clear to send (RTS/CTS) mechanism. This joint model enables us to analyze the throughput, transmission time and energy consumption of the network and to optimize parameters such as the number of WGs per WGN required to cover whole surveying area.

Furthermore, in unsaturated traffic model, it is required to find the probability of being idle. To calculate this probability, a buffer of size B is proposed in the WG and it is modeled as a D/M/1/B queue. It is worth mentioning that D/M/1/B is not observed in real applications, in particular, related to networks. This queue is used for the first time in this work. The reason is that this model is suitable for the scenario at hand, i.e., deterministic packet arrivals (seismic data is recorded at regular intervals) and random departure (communication between WG and WGN is carried out using CSMA/CA). This is in contrast to the previous works, in which the idle probability is either taken as input to the MAC model, i.e., considered to be known [11], or calculated using assumption of small buffer size with random arrivals [22].

Moreover, this work proposes to use IEEE 802.11af standard for communication between WGs and WGN. This standard operates in TV bands to achieve the maximum possible range and low power consumption among IEEE 802.11 family.

While many papers analyzed a certain functionality of IEEE 802.11 based network, the authors are not aware of any work that has performed cohesive analysis of the MAC, PHY and D/M/1/B model for seismic network presented in this work. In summary, unlike [1], the main contributions of this paper are the following:

1) Enhancing the MAC layer model by representing a buffering process in the wireless geophone with

D/M/1/B queueing model. Furthermore, the analytical expressions for the throughput, transmission time and energy consumption are derived using MAC, PHY and D/M/1/B queue model and shown to be useful for designing the seismic acquisition network without extensive simulations. The analytical expressions enables us to optimize the number of WGs per WGN and transmission time which are important factors for seismic acquisition system.

2) The analysis is done by considering IEEE 802.11af standard, which is proposed for the WG to WGN communications. This standard uses the TV white spaces for communication. The reason for considering these bands is to achieve larger transmission range with low power consumption, which reduces the required number of WGNs. The maximum range for this standard is 1 km.
3) The MAC model in [18] is extended for the RTS/CTS mode. This solves the hidden node problem and increases the throughput, since the collision only occurs on short RTS frames. Furthermore, more precise PHY error probability is provided by considering various path-loss models, modulation schemes, encoding schemes, noise within the hardware, and interference caused by neighboring WGNs.
4) In order to cover the whole seismic surveying area, frequencies allocated to the WGN are reused in a regular pattern. The joint MAC and PHY layer modeling together with queueing model enables us to analytically derive the interference due to frequency resuse and investigate its effect. Finally, cell sectoring is introduced to reduce the collision domain of CSMA/CA and to decrease the interference.

The rest of this paper is organized as follows. Section II is devoted to the seismic data acquisition network. Analytical models of MAC, PHY and buffering process are presented in Section III, and expressions of throughput, transmission time and energy are derived in Section IV. Analysis of energy consumption is carried out in Section V, whereas Section VI discusses the interference noise modeling and mitigation. Results are presented in Section VII, and finally, Section VIII draws the conclusions.

II. WIRELESS SEISMIC ACQUISITION NETWORK

This section presents the seismic network topology, MAC protocol for wireless interface and transmission channels.

A. DEPLOYMENT OF GEOPHONES

There are various layouts for the geophones in the seismic survey field; however, the orthogonal layout/placement, shown in Fig.1a, is the most common. For such placement in a typical field, there are around 480 WGs, at distance of 25 meters along inline direction, whereas 30 such lines of geophones are placed at distance of 200 meters along crossline direction. Total inline distance and crossline distances are 12 and 6 km, respectively. These facts and

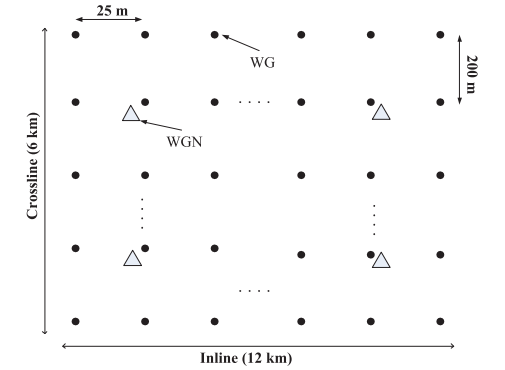

(a)

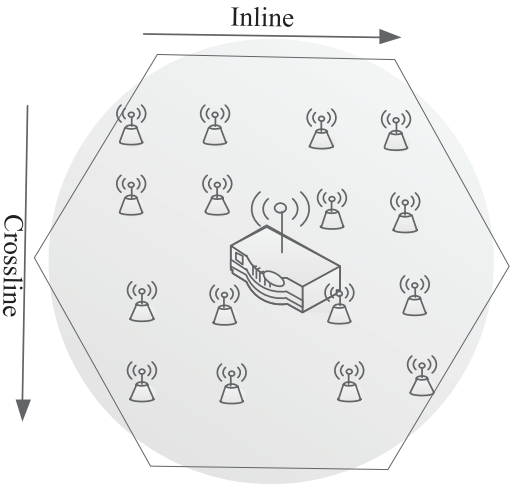

(b)

FIGURE 1. (a) Orthogonal geophone placement in a survey area, (b) A cell with wireless geophones and a wireless gateway node.

parameters are obtained from leading oil and gas companies in the Middle East. The geophones considered in this work are assumed to be equipped with a wireless interface. Furthermore, a centralized network is assumed, in which WGNs are placed in between geophone lines in such a way to cover all the surveying area (see Fig. 1a). Each WG sends its collected data to the WGN to which it is connected. One cell (serving area) of WGN with connected WGs is shown in Fig. 1b. All WGNs transmit received data to the data collection center for storage. The medium to transmit the data from WGN to the data collection center can be wired or wireless. However, this stage of transmission is beyond the scope of this work.

Since, the acquired seismic data is very important, a buffer capacity is necessary in wireless geophones in order not to drop packets. For this purpose, D/M/1/B queueing model is proposed, for the first time, as packets arrive at regular fixed intervals and leave the queue in a random fashion.

B. MAC PROTOCOL

In the IEEE 802.11 standard, the fundamental medium access mechanism is called distributed coordination function (DCF).

TABLE 1. Propagation model.

Model	Path-loss (PL) expression at distance d	Description
Free-space path-loss	$PL(d) = 20log_{10}d + 20log_{10}4\pi - (10log_{10}G_t + 10log_{10}G_r + 20log_{10}\lambda_w)$	Analytical model, assumes no obstacles between transmitter and receiver and valid for distance larger than Fraunhofer distance. G_t and G_r are the gains of transmit and receive antennas, receptively, and λ_w is the wavelength.
Two-ray	$PL(d) = 40log_{10}d - (10log_{10}G_t + 10log_{10}G_r + 20log_{10}h_{WGN} + 20log_{10}h_{WG})$	Analytical model, takes into account the LOS and ground-reflected signal. The free-space path-loss is used for distances less than crossover distance $d_c = \frac{4\pi h_{WG}h_{WGN}f_c}{c}$, where f_c is the carrier frequency and $c = 3 \times 10^8$ m/s. h_{WG} and h_{WGN} are the antenna heights for WG and WGN, respectively.
Egli model	$PL(d) = 40log_{10}d - (10log_{10}G_t + 10log_{10}G_r + 20log_{10}h_{WGN} + 20log_{10}h_{WG} + 10log_{10}\zeta)$	Analytical model, takes into account the rough terrain. $\zeta = (40/f_{cm})^2$ and f_{cm} is carrier frequency in MHz
One-slope log-normal	$PL(d) = PL(d_0) + 10nlog_{10}(d/d_0) + X_\sigma$	Empirical model, captures the effect of propagation mechanisms. n is the path-loss exponent, X_σ is the shadowing term, and $PL(d_0)$ is found from the free-space path-loss model at $d_0 = 1m$.
Two-slope path-loss	$PL(d) = PL(d_0) + 10n_1log_{10}(d/d_0) + X_{\sigma_1}$ for $d < d_{BP}$ and $PL(d) = PL(d_0) + 10(n_1 - n_2)log_{10}(d_{BP}) + 10n_2log_{10}(d) + X_{\sigma_2}\}$ for $d \geq d_{BP}$	Empirical model, accuracy is further increased by using multiple break points. The breakpoint distance is $d_{BP} = 4h_{WG}h_{WGN}f_c/c$.

This random access scheme is based on CSMA/CA mechanism.

In DCF mode, the CSMA/CA algorithm adopts a binary exponential backoff mechanism to limit collisions and control the transmission from various stations/WGs. This scheme mainly depends on a parameter called contention window, w_i. The number of backoff slots, i.e., how many slots a WG has to wait before it again assess the channel availability, is chosen randomly from the range 0 to $w_i - 1$. For the first transmission attempt, the value of w_1 is set to CW_{min}. For each retransmission attempt, if the transmission is unsuccessful (due to the collision or transmission error), the value of w_i is doubled until it reaches its maximum value, i.e., $CW_{max} = 2^m CW_{min}$, where m is the maximum number of backoffs. Mathematically, $w_i = 2^i CW_{min}$ for $0 \leq i \leq m$, and $w_i = 2^m CW_{min}$ for $i > m$. When a WG is ready to transmit some frames, it starts the backoff timer with a randomly selected number in the range $[0, w_i]$. The timer is decremented as long as the channel is sensed idle. If a transmission by another WG is detected, then the timer is frozen and reactivated upon sensing the channel to be idle again for more than distributed interFrame space (DIFS) time period. After the backoff counter counts down to 0, the packets are transmitted in the next time slot.

A positive acknowledgement (ACK) is sent to the WG, upon successful reception of a packet at the destination and waiting for a period of time called short interFrame space (SIFS). Since the duration of SIFS (plus the propagation delay) is shorter than the DIFS, no other WG senses the channel idle. If ACK is not received in the specified duration (ACT_time) or a different packet transmission is detected by the WG, then it reschedules the transmission according to the backoff mechanism explained above. The above described two-way handshaking technique is called the basic access mechanism.

DCF also defines a four-way handshake procedure known as RTS/CTS. In this technique, if a WG wants to transmit a packet, it performs the backoff procedure explained above, senses the channel for DIFS and sends a short frame called RTS frame. The receiving node (WGN), after receiving the RTS, respond with a CTS frame. Upon successful reception of CTS, the transmitting WG sends the packet. The RTS and CTS frames contains the information about the packet duration. Therefore, stations that hear the RTS or CTS updates the network allocation vector (NAV), which contains the information about the duration of time the channel remains busy. Hence, a WG that is hidden from the transmitting WG, delays its transmission and avoids possible collision. This technique is effective when large packets are involved in the transmission, since the collision only occurs on the RTS frames and is detected by the transmitting stations if the CTS frame is not received. This technique manages to solve the hidden node problem and is considered in our work.

C. CHANNEL MODELS

In [18], a time-varying Rayleigh fading channel is assumed for calculation of the PHY layer errors. However, this channel model is not suitable for our case. Firstly, it is not appropriate for TV bands. Secondly, it considers only non-line-of-sight (NLOS) with no dominant path, however, chances of line-of-sight (LOS) is high for seismic wireless systems. Finally, it models the Doppler effect caused by mobile reception, transmission or scatterers that introduces time-dependence to the channel. In our case reception and transmission is not mobile. Hence, the aim is to calculate more precise PHY layer error probability and hence, more accurate throughput, transmission time, and energy consumption using proper channel models. There are quite a few propagation channel models in the literature which are proposed/validated for near-ground communication in very high frequency/Ultra high frequency (VHF/UHF) bands [26]–[28]. These models, summarized in Table 1, are suitable for our scenario.

III. ANALYTICAL MODELS FOR MAC LAYER, PHY LAYER AND BUFFERING PROCESS

Figure 2 represents overall communication process to wirelessly transmit the acquired data from WG to WGN. The transmit buffer and the medium access module is modeled as system of Markov chains based on the source traffic model.

The IEEE 802.11 MAC model used in this work is inspired from Bianchi's [10] model and its extended unsaturated

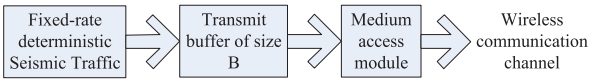

FIGURE 2. A block diagram representing system of Markov chains for WG-WGN communication process.

counterpart [18]. The MAC model presented here captures the effect of the WG's backoff stage, the retransmission counter, the idle stage and the physical channel. As a contribution, a D/M/1/B queueing model is also inserted into the MAC model to represent the buffering process at each WG. The reason for using a D/M/1/B queueing model is that the input to the buffer of the WG is deterministic with fixed arrival rate, and output is random (due to exponential backoff). On one hand, the MAC Markov model is used to determine the steady state probability of sensing the channel to be idle for transmitting a frame, the probability of collision if more than one WG transmits in the same time slot, and the probability of failure due to constraints of the physical layer. On the other hand, the D/M/1/B queueing model facilitates finding the performance parameters, e.g, throughput, and transmission time. Specifically, the queueing model is used to find idle state probability. In the following subsections, details about the MAC model, the PHY model, and the D/M/1/B queueing model are presented.

A. MAC LAYER MODEL

The generalization of the analytical MAC model of slotted CSMA/CA mechanism for the IEEE 802.11 is presented in [18]. In this work, this model is extended to RTS/CTS mechanism along with introduction of D/M/1/B queue.

This work considers a scenario of N contending WGs that send the data to a sink. Suppose, the probability that a WG sends a frame in the randomly selected time slot, the collision probability, and the probability of transmission failure are denoted as τ, P_{col}, and P_{fail}, respectively. The method presented here aims to solve the non-linear system of equations representing τ, P_{col} and P_{fail} together with the estimation of the idle probability, p_0. The idle probability is the probability of going back to the idle state if the buffer is empty by taking into account the offered load at each WG, i.e, λ. Consequently, our model enables the MAC model to determine this probability based on the arrival rate. Note that the capture effect in which a WG, with relatively high SNR, captures the channel in case of simultaneous multiple transmission, is not considered here. The reasons are: the RTS/CTS mode is insensitive to the capture, the transmission time is not influenced by the capturing effect and finally, capturing effect is only feasible to the indoor environment.

The IEEE 802.11 MAC discrete 2D Markov chain model is represented in Fig. 3, which shows the states and the transition probabilities. Fig. 3 is based on the following observation:

- There is an idle stage and backoff stages $(i, 0)$ to $(i, w_m - 1)$, $\forall i = 0, \ldots, m$. The state probability of backoff stage (i, j) is represented by $b_{i,j}$.

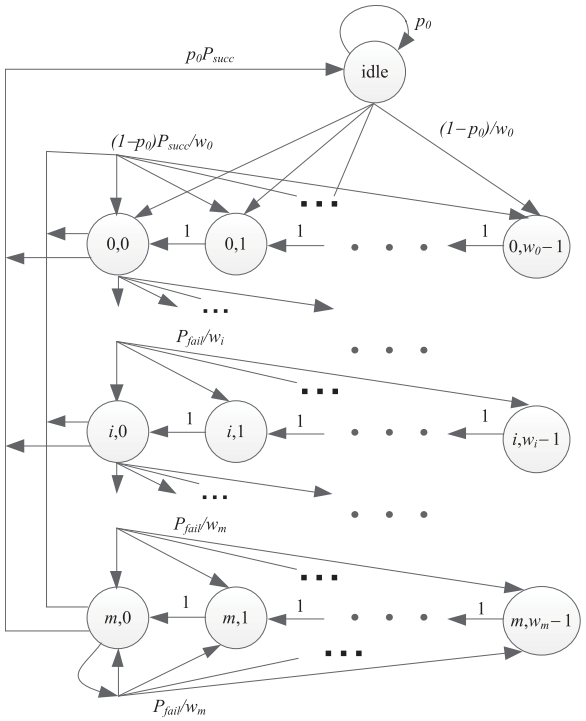

FIGURE 3. IEEE 802.11 MAC Markov chain model taking into account the transmission errors.

- The backoff counter is decremented with probability 1 at the beginning of each time slot.
- After a successful packet transmission in a time slot, if a WG has a packet in buffer to transmit then it starts the transmission from backoff stage 0 with probability $1 - p_0$.
- After each unsuccessful transmission (either due to packet collision or transmission error due to channel), the backoff stage is incremented to a new contention stage with probability P_{fail}/w_i. This increment seizes at backoff stage m, where WG keeps on trying with same contention window unless packet is successfully transmitted.
- If after a successful transmission, the buffer is empty then WG transits in the idle state waiting for a new packet.

The probability of successful transmission P_{succ} is the probability of having no collision and transmission errors and given as

$$P_{succ} = (1 - P_{phy})(1 - P_{col}), \tag{1}$$

where P_{phy} and P_{col} are the probability of transmission error due to the wireless channel and probability of collision, respectively, and $P_{fail} = 1 - P_{succ}$. The probability that a WG sends a frame in the randomly selected time slot, τ, is given as (see Appendix A), (2), as shown at the bottom of the next page, where m is the maximum number after which the backoff timer is seized. The collision probability, that is needed to compute P_{fail}, can be found by considering that the packet from the transmitting WG encounters a collision when at least $N - 1$ remaining WGs attempt to transmit

simultaneously. Hence, the collision probability is given as $P_{col} = 1 - (1-\tau)^{N-1}$.

B. PHY LAYER MODEL

Next, the PHY channel error probability, i.e., P_{phy} required in (1) is derived. In [18], a Rayleigh fading channel is assumed for calculation of PHY layer errors. In this work, all the aspects of PHY layer are considered to calculate P_{phy}, such as, modulation and encoding schemes, path-loss, and real environment channel for VHF/UHF band.

The PHY layer of the IEEE 802.11af standard is based on Orthogonal Frequency Division Multiplexing (OFDM) and uses Binary Phase Shift Keying (BPSK), and M-Quadrature Amplitude Modulation schemes (M-QAM) with $M = 4$, 16, 64 or 256. The probability of successful packet transmission on the PHY channel $P_{succ,phy}$ can be expressed as

$$P_{succ,phy} = (1 - P_{data})(1 - P_{ACK}), \tag{3}$$

where P_{data} and P_{ACK} are the probability of transmission error for packet and acknowledgement (ACK), respectively. The ACK frame is much smaller than the data frame and is transmitted at lowest rate (1.8 Mbits/s using BPSK). Hence, its transmission error probability is very low and can be ignored. Same is the case with RTS and CTS frames. Therefore, $P_{succ,phy} \approx 1 - P_{data}$. The probability of packet loss due to transmission error can be expressed as

$$P_{phy} = 1 - P_{succ,phy} = P_{data}. \tag{4}$$

The probability of transmission error for data packet is given as

$$P_{data} = 1 - \{P_R(H_{PHY})\}\{P_R(H_{MAC} + L_b)\}, \tag{5}$$

where H_{PHY}, H_{MAC}, and L_b are the PHY header, MAC header, and frame payload length in bytes. $P_R(H_{PHY})$ and $P_R(H_{MAC}+L_b)$ are the transmission success probability of the PHY header and data plus MAC header, respectively, given by [33] for various packet encoding as

$$P_R(H_{PHY}) = (1 - P_b)^{8H_{PHY}}, \tag{6}$$

and

$$\begin{aligned}
\text{NRZ}: \; & P_R(H_{MAC} + L_b) = (1 - P_b)^{8(H_{MAC}+L_b)} \\
\text{4B5B}: \; & P_R(H_{MAC} + L_b) = (1 - P_b)^{10(H_{MAC}+L_b)} \\
\text{Manchester}: \; & P_R(H_{MAC} + L_b) = (1 - P_b)^{16(H_{MAC}+L_b)} \\
\text{SECDED}: \; & P_R(H_{MAC} + L_b) = \{(1 - P_b)^8 \\
& \quad +8P_b(1-P_b)^7\}^{3(H_{MAC}+L_b)}
\end{aligned} \tag{7}$$

where non-return-to-zero (NRZ), 4-bits-to-5-bits (4B5B), Manchester, and single error correction and double error detection (SECDED) are the encoding schemes, and P_b is the probability of bit error.

In the IEEE 802.11af standard, OFDM is used at the PHY layer. Therefore, the received OFDM symbol $\mathcal{Y}$ is mathematically written as $\mathcal{Y} = \mathcal{H}\mathcal{X} + \mathcal{N}$, where $\mathcal{X}$ is the transmitted OFDM signal, $\mathcal{N}$ is the noise vector, $\mathcal{H} = diag(\bar{H}) = \mathbf{FhF}^*$ is the diagonal channel matrix, $\mathbf{F}$ is the FFT matrix, $\mathbf{h}$ is the channel impulse response, and $(.)^*$ is the Hermitian conjugate. At k^{th} frequency bin, the received signal can be written as $Y(k) = \bar{H}(k)X(k) + N(k)$, where $X(k)$ is the transmitted modulated symbol, $\bar{H}(k)$ is the channel effect and $N(k)$ is noise corresponding to k^{th} frequency bin.

Now, considering the OFDM model and static channel $\mathbf{h}$ (Table 1), P_b can be computed as [34]

$$\begin{aligned}
\text{BPSK}: \; & P_b = Q(\sqrt{2\gamma_b}) \\
M-\text{QAM}: \; & P_b \\
& = \frac{4}{K}\left(1 - \frac{1}{\sqrt{M}}\right) Q\left(\sqrt{\frac{6}{2(M-1)} K\gamma_b}\right) \\
& \quad \times \left[1 - \left(1 - \frac{1}{\sqrt{M}}\right) Q\left(\sqrt{\frac{6}{2(M-1)} K\gamma_b}\right)\right]
\end{aligned} \tag{8}$$

where $Q(.)$ is the Q-function which is found from lookup table [34], $\gamma_b = E_{b,r}/N_0$ is the received energy (Joules) per bit to noise power spectral density (Watt/Hz) ratio, and $K = log_2(M)$. To find the bit error probability from (8), γ_b is required, which can be related to the transmitted energy per bit, however, commercial radios do not provide this value, rather the transmitted power is provided. Hence, the relation of the transmitted power to γ_b is presented next.

The received energy per symbol to noise power spectral density ratio at the output of the receiver, i.e., $\gamma_s = E_{s,r}/N_0$ is given as, $\gamma_s = \frac{|\bar{H}(k)|^2 E_s}{N_0}$, where E_s is the transmitted energy per symbol and $\frac{E_s}{N_0} = \frac{C_s}{P_N} T_s B$, where B is the channel bandwidth (Hz), T_s is the symbol duration and C_s/P_N is the transmitted signal power to noise power ratio (power is in watt). Since, the symbol duration is related to bit duration as $T_s = log_2(M)T_b$, where $T_b = 1/R$ and R is data rate, therefore, $\gamma_b = \gamma_s/K$ to be used in (8). The noise power P_N can be classified as, environmental noise (noise due to sources outside the receiver) P_{NE}, interference noise (created from other users) P_{NI} and receiver noise factor (due to noise generated by electronic components) P_{NR}, i.e., $P_N = (P_{NE} + P_{NI})P_{NR}$. The noise factor P_{NR} (called as noise figure when expressed in dB) measures the degradation of the SNR caused by components in the receiver. The noise figure of an 802.11 receiver varies from 4 to 10 dB. Details about the interference noise is presented in Section VI. To conclude, the probability of

$$\tau = \frac{2(1 - 2P_{fail})(1 - p_0)}{(1 - p_0)[(w_0 + 1)(1 - 2P_{fail}) + w_0 P_{fail}(1 - (2P_{fail})^m)] + 2p_0(1 - P_{fail})(1 - 2P_{fail})} \tag{2}$$

transmission error P_{phy} depends on modulation and encoding schemes, interference, environmental and receiver noise.

C. D/M/1/B QUEUE MODEL

For equation (2), the idle probability p_0 was taken as input in the previous studies, e.g., see [11]. Furthermore, an approximate analysis is presented to calculate the idle probability in [22] with the assumption of a small size buffer, Poisson arrival, heterogeneous traffic and empty inter-arrival queue. These assumptions are scenario specific, and hence, not suitable for the analysis of seismic data acquisition system. Hence, in this work, the idle probability is found by considering a D/M/1/B queue model to represent the buffer in each WG.

In D/M/1/B queueing model (state transition diagram is shown in Fig. 4), packets arrive at regular fixed intervals, however, leave the queue in a random fashion. Assuming that exactly one packet arrive in the queue after n^{th} time step, i.e., nt, where one time step is equal to t sec. Furthermore, assume that the probability that a packet leaves the queue in one time step is p_l, and hence, the probability that packet does not leave is $p_{nl} = 1 - p_l$. In Fig. 4, each column corresponds to the number of packets in queue, i.e., the j^{th} column state probabilities $s_{0,j}$ to $s_{n-1,j}$ shows the particular occupancy of the queue indicating there are j packets in the queue. The total number of columns J represents the size of queue and the number of rows n corresponds to number of time steps between packet arrivals. The last row is the state when packet arrives, while the leftmost and rightmost columns corresponds to the empty queue and full queue, respectively. This D/M/1/B queue model is inspired from [23], however, here it is extended to the general form by using the arbitrary number of queue size and time steps. Furthermore, in order to find the state probabilities, an iterative procedure is used in this work.

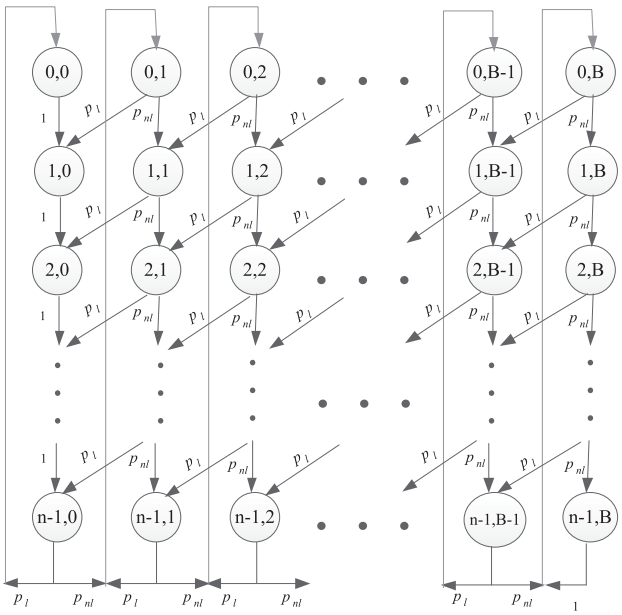

FIGURE 4. State transition diagram of D/M/1/B discrete-time queue.

The state vector $\mathbf{s}$ can be written in the form of B sub-vectors as $\mathbf{s} = [\mathbf{s}_0, \mathbf{s}_1, \ldots, \mathbf{s}_B]^T$, where T is the transposition operator. The sub-vector $\mathbf{s}_j$ (corresponds to j^{th} column) is given by $\mathbf{s}_j = [s_{0,j}, s_{1,j}, \ldots, s_{n-1,j}]^T$. Corresponding to the state vector $\mathbf{s}$, the 1-step transition matrix $\mathbf{P}$ has a dimension of $n(B+1) \times n(B+1)$. It is easy to write the transition matrix $\mathbf{P}$ in a composite matrix of dimension $(B+1) \times (B+1)$ as given in Appendix B.

From the transition matrix, the distribution vector $\mathbf{s}$ at the steady-state can be found from the following two equations

$$\mathbf{Ps} = \mathbf{s}, \tag{9}$$

$$\mathbf{1s} = 1, \tag{10}$$

where $\mathbf{1}$ is row vector of all 1s. The solution for the distribution vector $\mathbf{s}$ is found in an iterative fashion. For this purpose, the iterative equations can be written from (9) as follows.

$$\mathbf{s}_0 = \mathbf{P}^{(1,1)}\mathbf{s}_0 + \mathbf{P}^{(1,2)}\mathbf{s}_1, \tag{11}$$

$$\mathbf{s}_j = \mathbf{P}^{(2,1)}\mathbf{s}_{j-1} + \mathbf{P}^{(2,2)}\mathbf{s}_j + \mathbf{P}^{(1,2)}\mathbf{s}_{j+1}, \quad j = 1, 2, \ldots, B-1, \tag{12}$$

$$\mathbf{s}_B = \mathbf{P}^{(2,1)}\mathbf{s}_{B-1} + \mathbf{P}^{(B+1,B+1)}\mathbf{s}_B. \tag{13}$$

The expressions (11)-(13) are solved iteratively as follows: Initially, assign value to each element in distribution vector $\mathbf{s}$ as $\frac{1}{n(B+1)}$. Then, iterate through the equations (11)-(13) and stop when the distribution vector converges. The idle probability p_0 is given by

$$p_0 = \sum_{i=0}^{n-1} s_{i,0}. \tag{14}$$

and the average queue size Q can be found as $Q = \sum_{i=0}^{n-1}\sum_{j=1}^{B} j s_{i,j}$.

In order to find the inputs (t and p_l) to this queue model, the mean arrival rate λ (which is known from the acquisition rate), and the mean departure rate μ (which is equal to $1/E[T_p]$) are needed. Using the arrival rate, the value of nt is calculated as $nt = \frac{1}{\lambda}$.

The queue leaving probability, p_l, can be calculated from the departure distribution, which is a Poisson process, i.e., $P(K = k) = \frac{(\mu t)^k exp(-\mu t)}{k!}$. Hence, probability that a packet does not leave the queue, p_{nl}, is zero event in t sec, i.e.,

$$P(K = 0) = exp(-\mu t) = p_{nl}. \tag{15}$$

The value of n is found to be 25 in Section VII-A.

IV. THROUGHPUT AND TRANSMISSION TIME EXPRESSIONS

Using the models presented in Section III, throughput and transmission time expression are derived in this section. From the discussion in Section III, it can be seen that the probabilities τ, P_{col}, and P_{fail} are related by a three non-linear system of equations that resulted from steady state probabilities and given by (16)–(18), as shown at the bottom of the next page.

The above-mentioned probabilities are computed using the *fsolve* function of MATLAB.

A. THROUGHPUT

The solution of the equations (16), (17), and (18) enables us to compute the WG's throughput, which is defined as the fraction of time used to transmit payload bits over the channel and is given as (19), as shown at the bottom of the page, where σ_s is the duration of time slot and $E[L]$ is the average packet payload duration. P_t is the probability that there is at least one transmission in the given time slot, while N WGs are contending and each transmit with probability τ, and is given by

$$P_t = 1 - (1-\tau)^N, \tag{20}$$

and P_s is the conditional probability of success given at least one WG transmit, i.e.,

$$P_s = \frac{N\tau(1-\tau)^{N-1}}{P_t}. \tag{21}$$

In (19), T_c, T_e, and T_s are time duration the channel is sensed busy due to collision, transmission time of the error affected frame, and the successful frame transmission time, respectively. These times are given as,

$$T_c = RTS + CTS_{timeout}, \tag{22}$$

$$T_e = RTS + SIFS + \tau_p + CTS + SIFS + \tau_p + H + L + ACK_{timeout}, \tag{23}$$

$$T_s = RTS + SIFS + \tau_p + CTS + SIFS + \tau_p + H + L + SIFS + \tau_p + ACK + DIFS + \tau_p, \tag{24}$$

where H is the PHY and MAC headers duration, L is the packet payload duration (assuming all WG frames have same length, i.e., $E[L] = L$), τ_p is the propagation delay, $ACK_{timeout}$ ($CTS_{timeout}$) is equal to $SIFS + \tau_p + ACK$ (CTS), and $DIFS$ ($SIFS$) is the waiting time of sender (receiver) before sending frame (acknowledgment). Here, transmission time of the error affected frame is calculated based on the assumption that CTS frame is much smaller than the data frame and transmitted at lowest rate (1.8 MHz using BPSK), hence its transmission error probability is very low. Note that, $E[L]$, T_c, T_e, T_s have same units for the normalized throughput. To get the throughput in bits/s, normalized throughput is multiplied by the data rate R. The throughput per WGN is NS.

B. TRANSMISSION TIME

The expected time taken to receive a packet successfully can be calculated from (19) and is given by (25), as shown at the botom of the next page.

From (25), it can be seen that the time consists of three components. The first term represents the time spent to successfully transmit a packet T_s. The second term represents the amount of time the channel is idle, and $\frac{(1-P_t)}{P_tP_s(1-P_{phy})}$ is the average number of idle slots per packet transmission. The third term represents the time wasted on the channel because of collision for each successful transmission and $\frac{(1-P_s)}{P_s(1-P_{phy})}$ is the average number of collisions per each successful transmission. Finally, the fourth term represents the average time spend on the channel due to transmission error and $\frac{P_{phy}}{(1-P_{phy})}$ is the average number of packet transmission errors per successful transmission.

Moreover, the total time to transmit the whole data acquired in β sec with acknowledgments is given as:

$$T = N\beta\lambda E[T_p], \tag{26}$$

where λ is the offered load in frames/s.

V. ENERGY CONSUMPTION OF A WG

One of the greatest limitation of the seismic network is the finite energy resource. Hence, it is important to thoroughly investigate the energy consumption by a WG. This will help to predict the battery life and further design the acquisition system efficiently. The total energy consumption in order to observe the successful transmission of a packet, ξ_T, can be written as

$$\xi_T = \xi_s + \xi_{idle} + \xi_c + \xi_{phy}, \tag{27}$$

where ξ_s, ξ_{idle}, ξ_c, and ξ_{phy} are energies utilized in transmitting the packet successfully, while being idle, when there are collisions and when packet transmission errors occur, respectively. These four terms correspond to the terms in (25) and, can be found by expanding T_s, T_c and T_e and defining ρ_{tx}, ρ_{rx} and ρ_{idle} as power consumption by WG for transmitting, receiving, and being idle, respectively.

The energy spent in transmitting the packet successfully ξ_s can be sub-divided into energy used for transmission (sending RTS and packet), reception (receiving CTS and acknowledgment) and being idle (during SIFS and propagation) and it is given as

$$\xi_s = \rho_{tx}(RTS + H + L) + \rho_{rx}(CTS + ACK) + \rho_{idle}(3SIFS + 4\tau_p + DIFS). \tag{28}$$

$$\tau = \frac{2(1-2P_{fail})(1-p_0)}{(1-p_0)[(w_0+1)(1-2P_{fail}) + w_0P_{fail}(1-(2P_{fail})^m)] + 2p_0(1-P_{fail})(1-2P_{fail})} \tag{16}$$

$$P_{col} = 1 - (1-\tau)^{N-1}, \tag{17}$$

$$P_{fail} = P_{col} + P_{phy} - P_{phy}P_{col}, \tag{18}$$

$$S = \frac{P_tP_s(1-P_{phy})E[L]}{(1-P_t)\sigma_s + P_t(1-P_s)T_c + P_tP_s(1-P_{phy})T_s + P_tP_sP_{phy}T_e} \tag{19}$$

The energy consumption due to collision ξ_c can be divided into the energy spent in sending a packet and being idle when CTS times out and it is given as

$$\xi_c = \frac{(1-P_s)}{P_s(1-P_{phy})}[\rho_{tx}(RTS) + \rho_{idle}(CTS_{timeout})]. \quad (29)$$

Similar to ξ_s, the energy consumed while there is physical layer transmission error ξ_{phy} consists of energy used in sending the RTS and data packets, receiving the CTS, and being idle (during SIFS, propagation and acknowledgment time out), i.e.,

$$\xi_{phy} = \frac{P_{phy}}{(1-P_{phy})}[\rho_{tx}(RTS+H+L) + \rho_{rx}(CTS) + \rho_{idle}(2SIFS + 2\tau_p + ACK_{timeout})]. \quad (30)$$

Finally, the energy consumption when being idle ξ_{idle} is

$$\xi_{idle} = \frac{(1-P_t)}{P_tP_s(1-P_{phy})}\rho_{idle}\sigma_s. \quad (31)$$

It will be interesting to define the energy efficiency as fraction of energy used to successfully transmit a packet, i.e.,

$$\eta_\xi = \frac{\xi_s}{\xi_s + \xi_{idle} + \xi_c + \xi_{phy}}. \quad (32)$$

For small number of WGs per WGN, the energy efficiency will be higher as less energy is consumed in collision and being idle.

The overall procedure of calculating required quantities is highlighted in flow chart (Fig. 5). This figure explains the procedure to calculate the throughput, transmission time, and energy consumption using MAC, PHY and D/M/1/B queueing model. The convergence is achieved when the mean square error between the values obtained from two successive iterations becomes equal to a predefined value, e.g., 10^{-6} in this work.

VI. INTERFERENCE MODELING AND MITIGATION

In this section, interference noise is modeled and then cell sectoring is presented for interference reduction.

A. INTERFERENCE NOISE

Interference noise is the result of frequency reuse in the neighboring cells (a cell is coverage area of a WGN). Considering the cluster size, C, of 4 and radius of each cell as r, there are 6 immediate interference neighboring cells (indicated by arrows) at a distance of $D = r\sqrt{3C}$ [24] as shown in Fig. 6a (far away interfering cells are not considered as their interfering signal is not significant). In CSMA, the probability of packet transmission by WG is τ. Therefore, the probability of having i interferers out of N WGs in a cell is

$$P_I = \binom{N}{i}\tau^i(1-\tau)^{N-i}. \quad (33)$$

Assuming that all the WGs transmit with the same power I_t and I_{r_i} is the average received power (interference) from i^{th} interferer in any cell from the neighboring 6 cells. Further, assume that the interference signal strength at any point decays as a power law of the distance separation between the transmitter and the receiver, i.e., $I_{r_i} = I_{t_0}\left(\frac{d_i}{d_o}\right)^{-n}$, where I_{t_0} is the power received at a close-in reference point in the far field region of the antenna, i.e., at a small distance d_o from the transmitting antenna. Here, d_i is the average distance of i^{th} interferer from the concern WG. Due to orthogonal geometry, the average d_i is equal to D, and consequently, $I_{r_i} = I_r$. Therefore, the average interference signal received from all the 6 neighboring cells can be written as

$$P_{NI} = I_r\left[\sum_{i=1}^{6N}\binom{6N}{i}\tau^i(1-\tau)^{6N-i}i\right]. \quad (34)$$

A closer look at (34) reveals that the term in bracket is mean/expectation of a binomial random variable with parameter τ and $6N$. Hence, (34) can be written in compact form as $P_{NI} = 6I_rN\tau$.

B. CELL SECTORING

Cell sectoring can be used to increase the capacity (in terms of number of WGs per WGN) and the performance (in terms of throughput) by keeping the cell radius unchanged. Sectoring uses several directional antennas instead of the omidirectional antenna at the WGN, hence, reducing the interference. Each sector has its own collision domain. Hence, due to the directional antennas the collision domain within the cell is also reduced (WGs now contend within a sector instead of a cell), achieving better throughput performance. By using directional antennas, a given cell will receive interference from only fraction of the available interfering cells. This technique of reducing interference and collision domain by using directional antennas is referred to as sectoring. The reduction factor for interference and collision domain depends on the amount of sectoring used. A normal practice in cellular systems is to partition a cell into three 120^o or six 60^o sectors. When sectoring is employed, the channels used in a particular cell are broken down into sectored groups and are used only within a particular sector. Assuming a scenario of four-cell reuse (Fig. 6a), for the case of 120^o the number of interfering cells is reduced from six to two. This is because only two of

$$E[T_p] = \frac{(1-P_t)\sigma_s + P_t(1-P_s)T_c + P_tP_s(1-P_{phy})T_s + P_tP_sP_{phy}T_e}{P_tP_s(1-P_{phy})} = T_s + \frac{(1-P_t)}{P_tP_s(1-P_{phy})}\sigma_s + \frac{(1-P_s)}{P_s(1-P_{phy})}T_c + \frac{P_{phy}}{(1-P_{phy})}T_e. \quad (25)$$

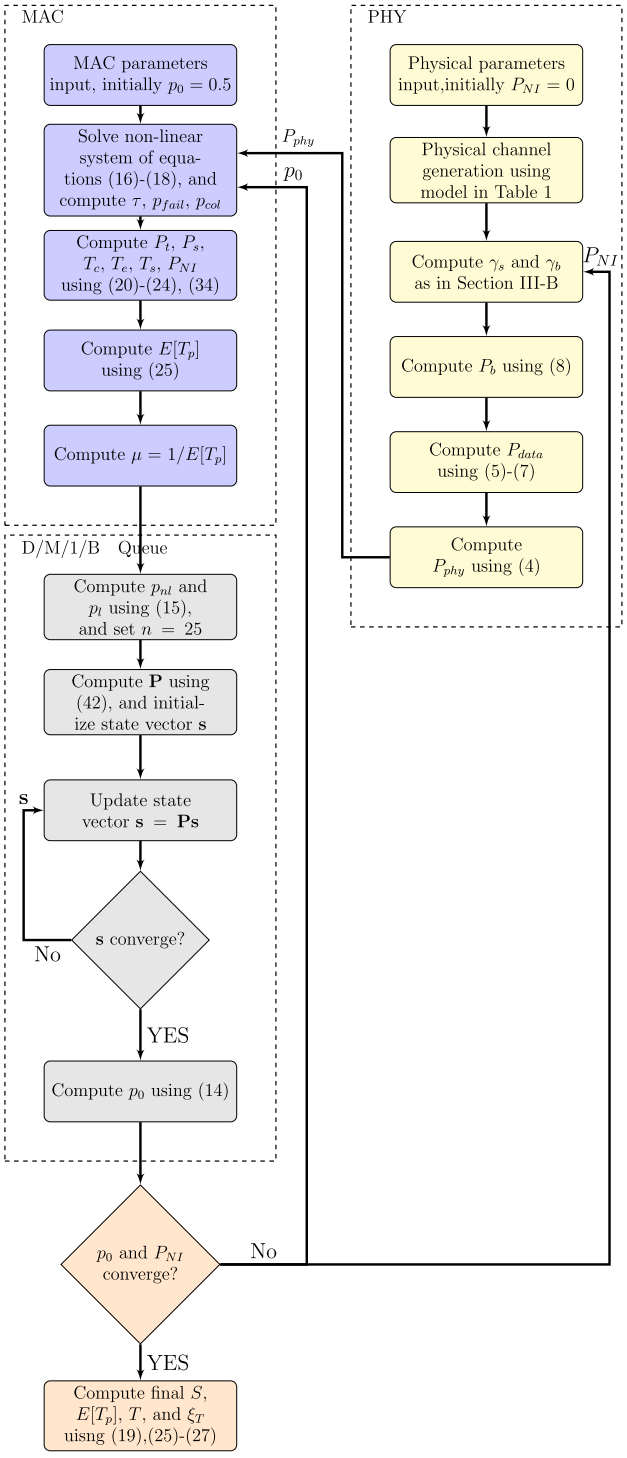

FIGURE 5. A combined MAC, PHY and queue model flowchart for computing throughput and expected time taken by a packet.

the six co-channel cells receive interference with a particular sectored channel group. Similarly, for the case of 60° the number of interfering cells is reduced from six to one as shown in Fig. 6b. Furthermore, the number of WGs per WGN causing interference will be reduced as well. Hence, for the

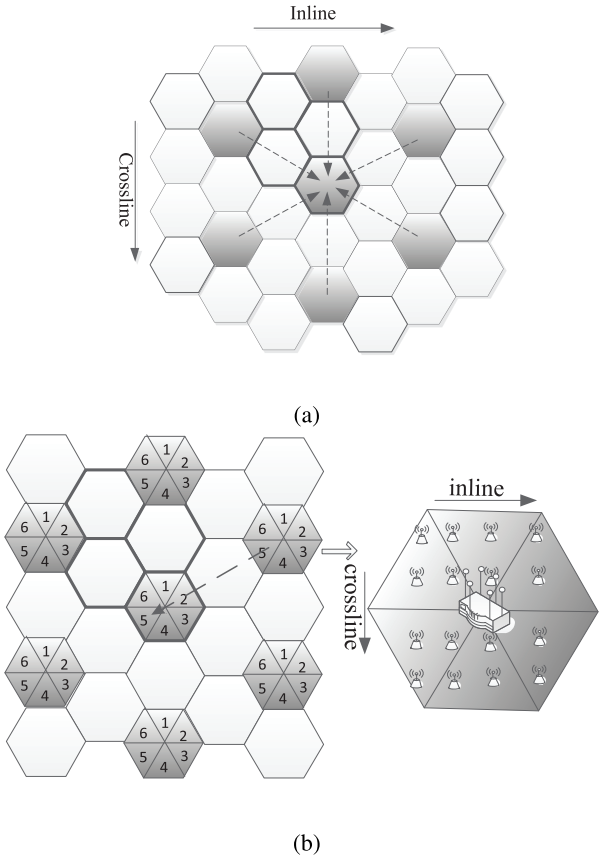

FIGURE 6. (a) Cluster size of 4 with 6 interfering neighbor cells, (b) Cluster size of 4 with 1 interfering neighbor cell's sector (interference to sector 5 of the middle cell is indicated by a dotted arrow).

60° sectoring case, $P_{NI} = \frac{I_r N \tau}{6}$. One of the drawback of the sectoring is increased number of handovers (switching from one to another cell/sector) in case of mobile network. However, thanks to our static environment that handover issue is not present.

VII. RESULTS AND DISCUSSION

In this section, the throughput and time for the transmission of data is investigated in wireless seismic acquisition system for various densities of geophones per WGN to cover the whole surveying field shown in Fig. 1a. The important questions here are: how many WGs can be served by one WGN and how many WGNs are required to serve the whole surveying area. To answer this question, various parameters are considered in the ensuing subsections.

A. PARAMETERS AND VALIDATION

The parameters used for our scenario are listed in Table 2 and 3. These adopted system parameters are based on the 802.11 standard [25]. The offered load is calculated as: the sampling frequency for the seismic acquisition systems is $f_s = 2$ kHz with 24 bits/sample, hence the data acquisition rate comes out to be 48 kbits/s per component of a three component (3C) geophone [5]. For 802.11, the MAC frame

TABLE 2. MAC and PHY layer parameters used in the study.

Layer	Parameter	Value
PHY	PHY header, H_{PHY}	128 bits
	Average propagation delay	1.7 μs
	Slot time	21 μs
	Antenna Gains, G_t, G_r	1, 1
	Transmit power, P_{tr}	20 dBm
	Power consumption, $\rho_{tx}, \rho_{rx}, \rho_{idle}$	0.3 W, 0.185 W, 0.066 W [29]
	Noise power, P_{NE}	5 dB
	Carrier frequency, f_c	470 MHz
	Channel bandwidth, B	6 MHz
	Noise Figure, P_{NR}	7 dB
	Path-loss exponents; n, n_1, n_2	3, 2.5, 3.5
	Shadowing standard deviation; σ, σ_1, σ_2	7 dB, 6 dB and 8 dB
	Height of antennas; h_{WG},h_{WGN},	1 m, 2 m
	Maximum Tx range	1000 m
	Data acquisition rate	48 kbits/s per component (144 kbits/s)
MAC	Smallest backoff window, CW_{min}	32
	Maximum backoff window, CW_{max}	1024
	MAC frame payload, L_b	9000 bits
	Offered load, λ	16 frames/s
	MAC header, H_{MAC}	192 bits
	ACK	112 bits + PHY header
	RTS	160 bits + PHY header
	CTS	112 bits + PHY header
	SIFS	16 μs
	DIFS	34 μs
	Queue size, B	50

TABLE 3. Modulation and data rates according to 802.11af.

Index	Modulation type	Coding rate	Data rate, R (Mbits/s).
1	BPSK	1/2	1.8
2	4-QAM	1/2	3.6
3	4-QAM	3/4	5.4
4	16-QAM	1/2	7.2
5	16-QAM	3/4	10.8
6	64-QAM	2/3	14.4
7	64-QAM	3/4	16.2
8	64-QAM	5/6	18.0
9	256-QAM	3/4	21.6
10	256-QAM	5/6	24.0

payload size is taken as 9000 bits/frame, therefore, the offered load is 16 frame/s. The recording phase duration is 14 s.

In D/M/1/B queue model, value of n is required. In order to find the suitable value of n, it is plotted against utilization for various values. Utilization is the ratio of the arrival rate to the departure rate, i.e., λ/μ. Figure 7a shows that for the higher values of n ($\geqslant 25$), the behavior of the D/M/1/B model is not changing. Hence, the value of n is taken as 25.

Next, the theoretical and simulation results are compared in Figs. 7b and 7c for all values of utilization. The simulations are carried out in Monte Carlo fashion assuming that the queue has deterministic arrival and Poisson departure. Based on these assumptions, the probability that queue is idle and the queue size for various values of utilization are plotted in Figs. 7b and 7c. These figures verified a close match between theoretical and simulated performances for all values of the utilization.

B. RANGE OF WGN

Figure 8a shows the mapping between the coverage radius of the WGN to the number of WGN required to cover the whole serving area and to the number of WGs served by a single WGN. It is direct to see that as the coverage range increases, the required number of the WGNs decreases.

Here, TV white spaces are considered for the transmission in order to have maximum possible coverage of WGN. The coverage range of 802.15.4 is 20 m, which is very small for our scenario. On the other hand, the recently proposed IEEE802.11af standard (that uses TV white spaces) has a maximum range of 1000 m. With 1 km of coverage range, the number of WGs per WGN are around 600 and 22 WGNs (Fig. 8a) are needed to serve the whole surveying area. This means that the maximum number of WGs supported by a WGN based on its coverage range is $N_r = 600$ WG.

C. AGGREGATE THROUGHPUT

Next, the throughput per WGN is shown in Fig. 8b. From this figure, it is concluded that there is a saturation point after

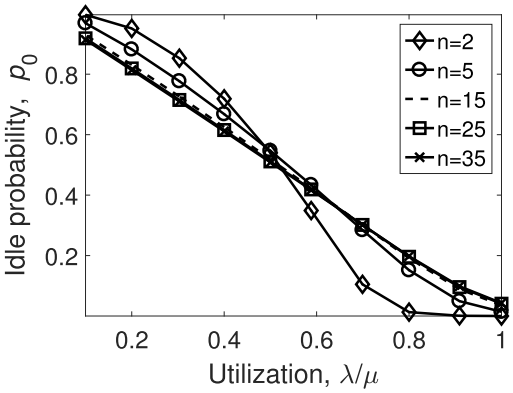

(a)

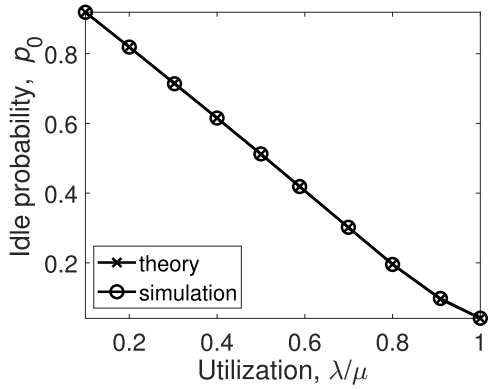

(b)

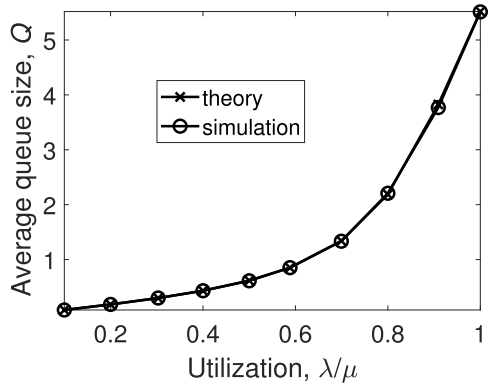

(c)

FIGURE 7. (a) Comparison of idle probability p_o verses utilization λ/μ for various values of n in D/M/1/B queueing model, (b) Comparison of idle probability p_0 for theoretical and simulated model, (c) Comparison of average queue size Q for theoretical and simulated model.

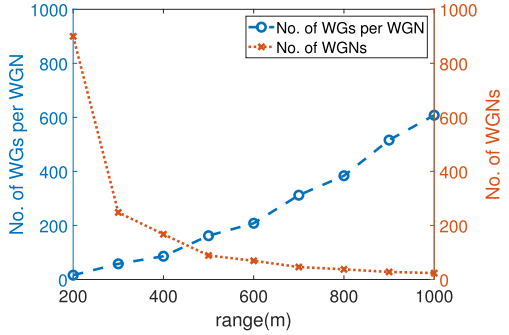

(a)

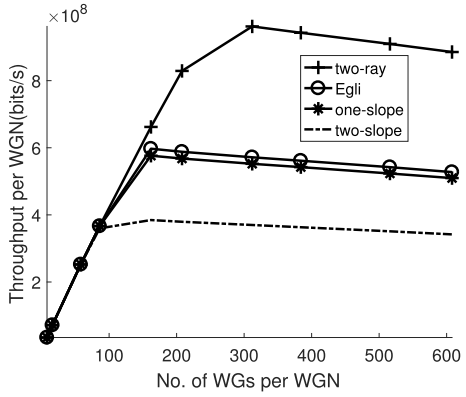

(b)

FIGURE 8. (a) Number of WGNs needed for the surveying area and Number of WGs per WGN versus the coverage radius of the WGN, (b) Throughput per WGN verses number of WGs per WGN for various channel models.

which the throughput starts decreasing. The reason is that the throughput depends on the number of WGs per WGN and collisions. When the number of WGs per WGN increases, throughput per WGN increases. However, due to the increase in the number of WG per WGN collision increases and consequently, throughput per WGN decreases. Hence, there comes a point where the decrease in throughput due to collisions overcomes the increase in throughput due to the increase in the number of WGs per WGN. This saturation point is very useful in the analysis and can be used to find the number of WGs that can be covered by a WGN so that the throughput is maximized. From this figure, it is concluded that the maximum value of throughput occurs at $N_{TH} = 312$ WGs per WGN for two-ray channel model. It can be noted from Fig. 8b that the effect of path-loss model is not noticeable when WGs are close to WGN.

D. TRANSMISSION TIME OF DATA

The timing diagram [30] for seismic data acquisition process is shown in Fig. 9a. It shows that data is recorded for 14 s. The acquisition process is repeated after 16 s. Hence, the time required to transmit the data from WG to WGN is investigated for various number of WGs supported by WGN.

Fig. 9b shows that number of WGs versus the transmission time to transfer the data from all WGs to the respective WGN. The total time to transmit the whole data acquired in 14s (total recording time) with acknowledgment by a WGN is given as: $T = N * 14 * 16 * E[T_p]$ (from (26)). The useful information about the transmission time in the figure can be use to optimize the number of WGs in a coverage area of

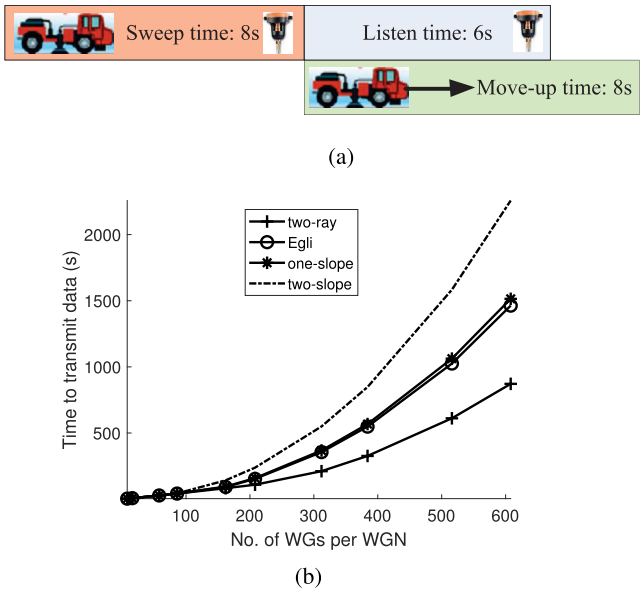

FIGURE 9. (a)Timing diagram for seismic data acquisition, (b) Time to transmit data versus number of WGs per WGN.

WGN. For example, a restriction on the time can be placed and calculate the number of WGs served by a WGN. The restriction is useful as the shooting and recording process for seismic acquisition is repeatedly done for days. For rest of the figures, one-slope channel model is used, unless otherwise stated.

E. MAC PAYLOAD SIZE

For the Figs. 8b and 9b, the MAC payload size was taken as 9000 bits. It will be interesting to see the effect of payload size on throughput. Figure 10a shows that as the MAC payload size increases, throughput increases for a fixed number of WGs. Therefore, the MAC maximum payload size of 18000 bits can be taken.

F. ENCODING

In all the previous results, NRZ encoding is used. It is interesting to see the effect of packet encoding schemes, as in (7), on throughput. Figure 10b shows that the NRZ encoding achieves the maximum throughput, since it does not have any redundant information. On the other hand, encoding method SECDED has the lowest throughput. The reason of less throughput of the encoding schemes as compared to NRZ is that they have redundant information for self clocking and/or bit error correction. Hence, throughput can be compromised for other advantages. The maximum number of WGs per WGN that give the maximum throughput is same for all the encoding schemes. Furthermore, for less number of WGs per WGN (<=100) the encoding performance is same.

G. MODULATION SCHEME

4-QAM modulation scheme with data rate of 3.6 Mbits/s is used for the throughput analysis in all the previous figures.

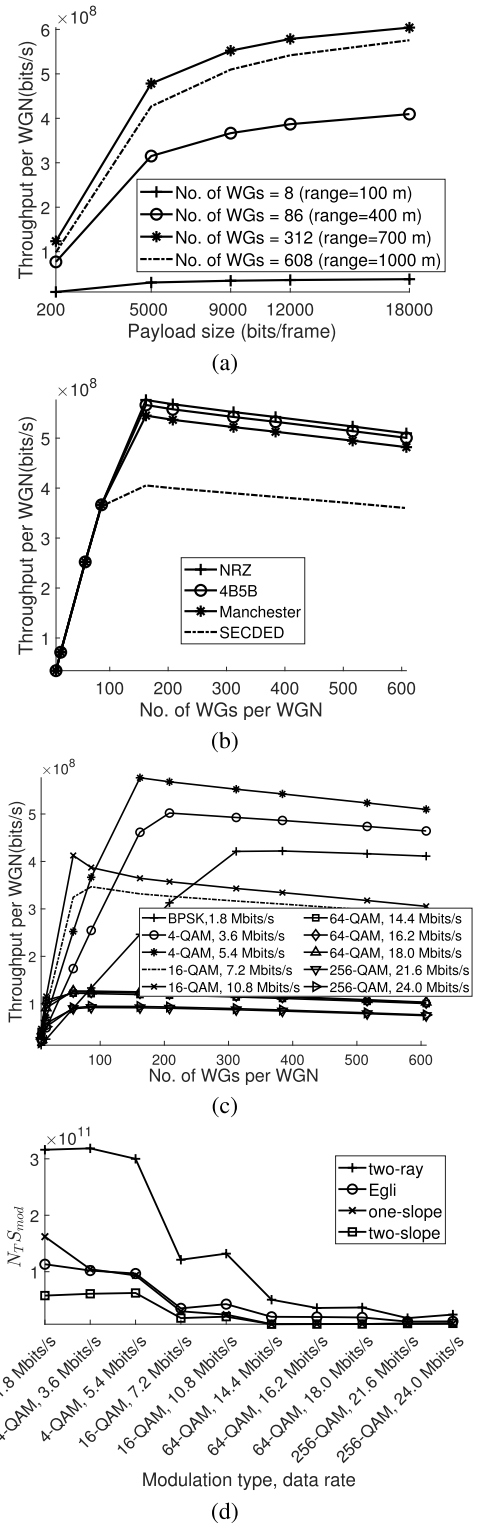

FIGURE 10. (a) Throughput per WGN versus MAC payload, (b) Throughput per WGN verses number of WGs per WGN for various encoding schemes, (c) Effect of modulation schemes and data rates on throughput per WGN, (d) Modulation schemes and data rates verses $N_T S_{mod}$.

In equation (8), probability of bit error is given for various modulation schemes. In reality, standards use adaptive modulation schemes, i.e., a modulation scheme is selected

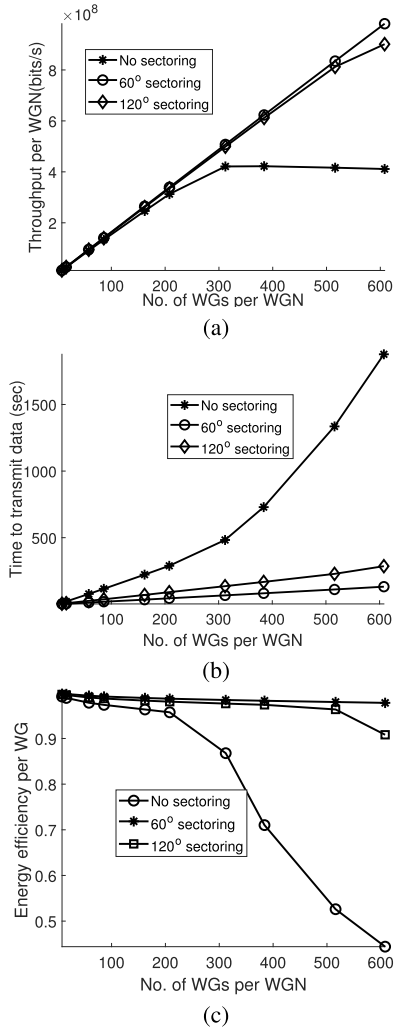

FIGURE 11. (a) Throughput per WGN for the case of 120° sectoring and 60° sectoring, (b) time required to send the data for the case of 120° sectoring and 60° sectoring, (c) Energy efficiency per WG verses number of WGNs.

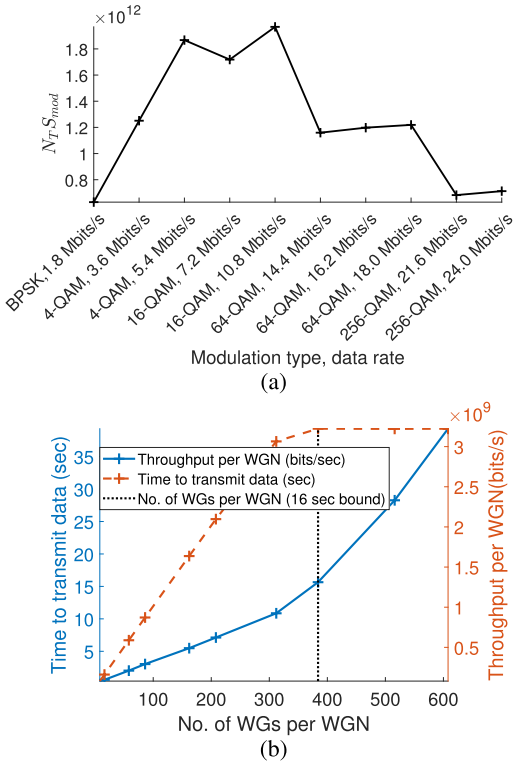

FIGURE 12. (a) Modulation schemes and data rates verses $N_T S_{mod}$, (b) time required to send the data and throughput per WGN. Other parameters used in this case are 16-QAM modulation (10.8 Mbits/s), NRZ encoding, payload size of 18000 bits, 60° sectoring and one-slope channel model.

based on the channel condition. The setup is evaluated for various modulation schemes and data rates given in Table 3. Figure 10c depicts the throughput for various modulation and data rates. It shows that as the number of bits per symbol is increased by using the higher order modulation scheme, the maximum number of WG per WGN decreases. However, the throughput increases up to 4-QAM with data rate of 5.4 Mbits/s and then decreases for higher order QAM. The reason for this behavior is as follows: when more bits per symbol are transmitted, throughput per WGN increases. On the other hand with more bits per symbol bit error rate also increases, which decreases the throughput. The aim is to select the modulation scheme and data rate that gives maximum throughput and maximum number of WGs per WGN among all the modulation schemes. For this purpose, the product of maximum throughput per WGN over the range of $1 - 1000$ m for a specific modulation scheme and data rate, S_{mod}, and the corresponding value of WGs per WGN, N_T, is plotted in Fig. 10d. The values of S_{mod} and N_T are obtained from Fig. 10c. It is concluded from Fig. 10d that BPSK with data rate of 1.8 Mbits/s gives best results for one-slope and Egli channel models, whereas 4-QAM with 5.4 Mbits/s and 7.2 Mbits/s are best for two-ray and two-slope channel models, respectively.

H. SECTORING

Next, the performance is measured using sectoring. The 120° and 60° sectoring are used. It can be seen from Fig. 11a, that using sectoring increases the throughput (due to reduce collision domain and less interference) and, hence, more WGs per WGN can be accommodated. Similarly the time required to send the data is tremendously reduced as shown in Fig. 11b,where BPSK with data rate of 1.8 Mbits/s is used.

I. ENERGY CONSUMPTION

Figure 11c depicts the energy efficiency per WGN, η_ξ. It can be noted from the figure that sectoring increases the energy efficiency tremendously. Since there are less collisions and interference in case of sectoring, therefore, the efficiency improves as compared to the no sectoring case. For 60^o sectoring, energy efficiency is almost close to one. In order to achieve even better performance in terms of energy efficiency, WGs with in a sector can be grouped together and a master WG can be selected to transmit data to WGN [32].

J. OPTIMUM NUMBER OF WGs PER WGN

The analysis presented above is useful for designing seismic wireless acquisition networks. For instance, 384 WGs can be assigned to one WGN in case of one-slope channel model. The value is obtained when the upper bound on the time is set to 16 seconds (sweep plus listen plus move-up time), i.e., WGs must finish sending data to respective WGN before the next shot. The other parameters used in this case are 16-QAM modulation (10.8 Mbits/s), NRZ encoding, payload size of 18000 bits, and 60° sectoring. These parameters are selected to get the maximum possible aggregated throughput. The results are shown in Figs. 12a and 12b.

VIII. CONCLUSION

In this work, a wireless seismic acquisition network is examined and investigated using Markov chain models. In particular, the MAC and PHY layer protocols are discussed for the transmission between WGs and WGN, and throughput, transmission time and energy consumption are analyzed. The proposed model incorporates the proper path-loss channel models, encoding and modulation schemes, and packet payload size. The buffer in a WG is modeled using D/M/1/B queue. It is shown that these results are useful for designing such wireless seismic acquisition networks, in particular, to find the optimal number of WGs served by a WGN, and the total number of WGNs to serve the whole surveying area. In order to have a minimum number of WGNs, the IEEE 802.11af standard is considered which have a maximum range of 1 km. Finally, sectoring is also introduced for maximizing the number of WGs per WGN and hence, minimizing the total number of WGNs needed. It is worth to mention here that the energy constraint, the timing constraint and the quick quality check (QC) required in wireless seismic acquisition are some of the issues in wireless acquisition that are open to research. Wires are also responsible for providing power to the geophones, hence an efficient energy system (possibly using energy harvesting technology) is needed for self-sustainable wireless geophone.

APPENDIX A
STEADY STATE PROBABILITIES AND τ

In this appendix, some results are repeated from [18] for the sake of self-containedness and clarity.

In order to get the closed form solution for the Markov chain, all the steady state probabilities are expressed as a function of $b_{0,0}$ and then the normalization condition is used, i.e., sum of all the state probabilities is equal to one, to find $b_{0,0}$.

From Fig. 3, it can be noted that

$$b_{i,0} = P_{fail}^{i} b_{0,0}, \ 1 \le i \le m-1, \tag{35}$$

$$b_{m,0} = \frac{P_{fail}^{m}}{1-P_{fail}}, \ i = m, \tag{36}$$

$$b_{idle} = \frac{p_0 P_{succ}}{1-p_0} \sum_{i=0}^{m} b_{i,0}, \tag{37}$$

$$\sum_{i=0}^{m} b_{i,0} = \frac{b_{0,0}}{P_{succ}}. \tag{38}$$

Owing to the Markov chain regularities, for $1 \le k \le w_i - 1$, we have

$$b_{i,k} = \frac{w_i - k}{w_i} \begin{cases} (1-p_0)P_{succ} \sum_{i=1}^{m} b_{i,0} & \\ +(1-p_0)b_{idle}, & i = 0 \\ P_{fail} b_{i-1,0}, & 1 \le i \le m-1 \\ P_{fail}(b_{m-1,0} + b_{m,0}), & i = m \end{cases} \tag{39}$$

The normalization condition, i.e., $\sum_{i=0}^{m} \sum_{k=0}^{W_i-1} b_{i,k} + b_{idle} = 1$, yields the equation for computation of $b_{0,0}$ as (40), shown at the top of the next page.

By taking into the fact that transmission starts when backoff counter reaches zero, τ is given (41), as shown at the top of the next page.

APPENDIX B
TRANSITION MATRIX P

The composite transition matrix $\mathbf{P}$ is given as

$$\mathbf{P} = \begin{bmatrix} \mathbf{P}^{(1,1)} & \mathbf{P}^{(1,2)} & \mathbf{0} & \cdots & \mathbf{0} & \mathbf{0} & \mathbf{0} \\ \mathbf{P}^{(2,1)} & \mathbf{P}^{(2,2)} & \mathbf{P}^{(1,2)} & \cdots & \mathbf{0} & \mathbf{0} & \mathbf{0} \\ \mathbf{0} & \mathbf{P}^{(2,1)} & \mathbf{P}^{(2,2)} & \cdots & \mathbf{0} & \mathbf{0} & \mathbf{0} \\ \vdots & \vdots & \vdots & \ddots & \vdots & \vdots & \vdots \\ \mathbf{0} & \mathbf{0} & \mathbf{0} & \cdots & \mathbf{P}^{(2,2)} & \mathbf{P}^{(1,2)} & \mathbf{0} \\ \mathbf{0} & \mathbf{0} & \mathbf{0} & \cdots & \mathbf{P}^{(2,1)} & \mathbf{P}^{(2,2)} & \mathbf{P}^{(1,2)} \\ \mathbf{0} & \mathbf{0} & \mathbf{0} & \cdots & \mathbf{0} & \mathbf{P}^{(2,1)} & \mathbf{P}^{(B+1,B+1)} \end{bmatrix} \tag{42}$$

where all the sub-matrices are of size $n \times n$ and given by

$$\mathbf{P}^{(1,1)} = \begin{bmatrix} 0 & 0 & \cdots & 0 & p_l \\ 1 & 0 & \cdots & 0 & 0 \\ 0 & 1 & \cdots & 0 & 0 \\ \vdots & \cdots & \ddots & \vdots & \vdots \\ 0 & 0 & \cdots & 1 & 0 \end{bmatrix},$$

$$\mathbf{P}^{(2,1)} = \begin{bmatrix} 0 & 0 & \cdots & 0 & p_{nl} \\ 0 & 0 & \cdots & 0 & 0 \\ 0 & 0 & \cdots & 0 & 0 \\ \vdots & \cdots & \ddots & \vdots & \vdots \\ 0 & 0 & \cdots & 0 & 0 \end{bmatrix},$$

$$\mathbf{P}^{(1,2)} = \begin{bmatrix} 0 & 0 & \cdots & 0 & 0 \\ p_l & 0 & \cdots & 0 & 0 \\ 0 & p_l & \cdots & 0 & 0 \\ \vdots & \cdots & \ddots & \vdots & \vdots \\ 0 & 0 & \cdots & p_l & 0 \end{bmatrix},$$

$$\mathbf{P}^{(2,2)} = \begin{bmatrix} 0 & 0 & \cdots & 0 & p_l \\ p_{nl} & 0 & \cdots & 0 & 0 \\ 0 & p_{nl} & \cdots & 0 & 0 \\ \vdots & \cdots & \ddots & \vdots & \vdots \\ 0 & 0 & \cdots & p_{nl} & 0 \end{bmatrix},$$

$$b_{0,0} = \frac{2P_{succ}(1-2P_{fail})(1-p_0)}{(1-p_0)[(w_0+1)(1-2P_{fail})+w_0P_{fail}(1-(2P_{fail})^m)]+2p_0(1-P_{fail})(1-2P_{fail})}. \tag{40}$$

$$\begin{aligned}\tau &= \sum_{i=0}^{m} b_{i,0} \\ &= \frac{2(1-2P_{fail})(1-p_0)}{(1-p_0)[(w_0+1)(1-2P_{fail})+w_0P_{fail}(1-(2P_{fail})^m)]+2p_0(1-P_{fail})(1-2P_{fail})}.\end{aligned} \tag{41}$$

$$\mathbf{P}^{(B+1,B+1)} = \begin{bmatrix} 0 & 0 & \cdots & 0 & 1 \\ p_{nl} & 0 & \cdots & 0 & 0 \\ 0 & p_{nl} & \cdots & 0 & 0 \\ \vdots & \cdots & \ddots & \vdots & \vdots \\ 0 & 0 & \cdots & p_{nl} & 0 \end{bmatrix}.$$

ACKNOWLEDGMENT

This article was presented in part at the IEEE International Symposium on Personal, Indoor and Mobile Radio Communications (IEEE PIMRC), Bologna, Italy, September 2018.

REFERENCES

[1] N. Iqbal, S. Al-Dharrab, A. Muqaibel, W. Mesbah, and G. Stuber, "Analysis of wireless seismic data acquisition networks using Markov chain models," in *Proc. IEEE 29th Annu. Int. Symp. Pers., Indoor Mobile Radio Commun. (PIMRC)*, Sep. 2018, pp. 1–5.

[2] S. Savazzi and U. Spagnolini, "Wireless geophone networks for high-density land acquisition: Technologies and future potential," *Lead. Edge*, vol. 27, no. 7, pp. 882–886, Jul. 2008.

[3] S. Savazzi and U. Spagnolin, "Synchronous ultra-wide band wireless sensors networks for oil and gas exploration," in *Proc. IEEE Symp. Comput. Commun.*, Jul. 2009, pp. 907–912.

[4] D. Freed, "Cable-free nodes: The next generation land seismic system," *Lead. Edge*, vol. 27, no. 7, pp. 878–881, Jul. 2008.

[5] S. Savazzi, U. Spagnolini, L. Goratti, D. Molteni, M. Latva-Aho, and M. Nicoli, "Ultra-wide band sensor networks in oil and gas explorations," *IEEE Commun. Mag.*, vol. 51, no. 4, pp. 150–160, Apr. 2013.

[6] R. Ellis, "Current cabled and cable-free seismic acquisition systems each have their own advantages and disadvantages–is it possible to combine the two?" *1st Break*, vol. 32, pp. 91–96, Jan. 2014.

[7] D. Crice, P. Flood, and E. Walthinsen, "Cableless seismic systems for near surface geophysics," in *Proc. Symp. Appl. Geophys. Eng. Environ. Problems*, Mar. 2015, pp. 465–468.

[8] X. Zhang, S. Zhang, J. Lin, F. Sun, X. Zhu, Y. Yang, X. Tong, and H. Yang, "An efficient seismic data acquisition based on compressed sensing architecture with generative adversarial networks," *IEEE Access*, vol. 7, pp. 105948–105961, 2019.

[9] S. Pollin, M. Ergen, S. C. Ergen, B. Bougard, L. V. Der Perre, I. Moerman, A. Bahai, P. Varaiya, and F. Catthoor, "Performance analysis of slotted carrier sense IEEE 802.15.4 medium access layer," *IEEE Trans. Wireless Commun.*, vol. 7, no. 9, pp. 3359–3371, Sep. 2008.

[10] G. Bianchi, "Performance analysis of the IEEE 802.11 distributed coordination function," *IEEE J. Sel. Areas Commun.*, vol. 18, no. 3, pp. 535–547, Mar. 2000.

[11] P. Park, P. Di Marco, P. Soldati, C. Fischione, and K. H. Johansson, "A generalized Markov chain model for effective analysis of slotted IEEE 802.15.4," in *Proc. IEEE 6th Int. Conf. Mobile Adhoc Sensor Syst.*, Oct. 2009, pp. 130–139.

[12] P. Chatzimisios, V. Vitsas, and A. C. Boucouvalas, "Throughput and delay analysis of IEEE 802.11 protocol," in *Proc. 3rd IEEE Int. Workshop Syst.-on-Chip Real-Time Appl.*, Oct. 2002, pp. 168–174.

[13] Z. Hadzi-Velkov and B. Spasenovski, "Saturation throughput–delay analysis of IEEE 802.11 DCF in fading channel," in *Proc. IEEE Int. Conf. Commun. (ICC)*, vol. 1, Mar. 2003, pp. 121–126.

[14] H. Zhai, Y. Kwon, and Y. Fang, "Performance analysis of IEEE 802.11 MAC protocols in wireless LANs," *Wireless Commun. Mobile Comput.*, vol. 4, no. 8, pp. 917–931, Dec. 2004.

[15] O. Tickoo and B. Sikdar, "Queueing analysis and delay mitigation in IEEE 802.11 random access MAC based wireless networks," in *Proc. IEEE INFOCOM*, vol. 2, Mar. 2004, pp. 1404–1413.

[16] H. Wu, Y. Peng, K. Long, S. Cheng, and J. Ma, "Performance of reliable transport protocol over IEEE 802.11 wireless LAN: Analysis and enhancement," in *Proc. 21st Annu. Joint Conf. IEEE Comput. Commun. Societies*, vol. 2, Jun. 2002, pp. 599–607.

[17] P. Raptis, A. Banchs, and K. Paparrizos, "A-simple-and-effective-delay-distribution-analysis-for-IEEE-802.11," in *Proc. IEEE 17th Int. Symp. Pers., Indoor Mobile Radio Commun.*, Sep. 2006, pp. 1–5.

[18] F. Daneshgaran, M. Laddomada, F. Mesiti, and M. Mondin, "Unsaturated throughput analysis of IEEE 802.11 in presence of non ideal transmission channel and capture effects," *IEEE Trans. Wireless Commun.*, vol. 7, no. 4, pp. 1276–1286, Apr. 2008.

[19] X. Cao, B. Yang, and Z. Song, "Performance analysis of hybrid MAC scheme with multi-slot reservation," *Electron. Lett.*, vol. 54, no. 4, pp. 250–252, Feb. 2018.

[20] P. Chatzimisios, A. C. Boucouvalas, and V. Vitsas, "IEEE 802.11 packet delay-a finite retry limit analysis," in *Proc. IEEE Global Telecommun. Conf. (GLOBECOM)*, vol. 2, Dec. 2003, pp. 950–954.

[21] P. K. Sahoo and J.-P. Sheu, "Modeling IEEE 802.15.4 based wireless sensor network with packet retry limits," in *Proc. 5th ACM Symp. Perform. Eval. Wireless Ad Hoc, Sensor, Ubiquitous Netw. (PE-WASUN)*. New York, NY, USA: ACM, 2008, pp. 63–70.

[22] D. Malone, K. Duffy, and D. Leith, "Modeling the 802.11 distributed coordination function in nonsaturated heterogeneous conditions," *IEEE/ACM Trans. Netw.*, vol. 15, no. 1, pp. 159–172, Feb. 2007.

[23] F. Gebali, *Analysis of Computer Networks*. Cham, Switzerland: Springer, 2015.

[24] T. Rappaport, *Wireless Communications: Principles and Practice*, 2nd ed. Upper Saddle River, NJ, USA: Prentice-Hall, 2001.

[25] C. Wang, H.-K. Lo, and S.-H. Fang, "Fairness analysis of throughput and delay in WLAN environments with channel diversities," *EURASIP J. Wireless Commun. Netw.*, vol. 2011, no. 1, p. 42, Dec. 2011.

[26] J. S. Seybold, *Introduction to RF Propagation*. New York, NY, USA: Wiley, Sep. 2005.

[27] Y. Huang, "Outdoor signal strength measurement at TV band and ISM band in otaniemi campus," M.S. thesis, School Elect. Eng., Dept. Commun. Netw., Aalto Univ., Espoo, Finland, 2013.

[28] S. Kurt and B. Tavli, "Path-loss modeling for wireless sensor networks: A review of models and comparative evaluations.," *IEEE Antennas Propag. Mag.*, vol. 59, no. 1, pp. 18–37, Feb. 2017.

[29] M. Ergen and P. Varaiya, "Decomposition of energy consumption in IEEE 802.11," in *Proc. IEEE Int. Conf. Commun.*, Jun. 2007, pp. 403–408.

[30] C. Bagaini, T. Bunting, A. El-Emam, and A. Laake, "Land seismic techniques for high-quality data," *Oilfield Rev.*, vol. 22, no. 2, pp. 28–39, 2010.

[31] J. C. Goswami, A. E. Hoefel, and H. Schwetlick, "On subsurface wireless data acquisition system," *IEEE Trans. Geosci. Remote Sens.*, vol. 43, no. 10, pp. 2332–2339, Oct. 2005.

[32] N. Iqbal, "Energy efficient architecture for wireless geophone networks," in *SEG Technical Program Expanded Abstracts 2019*. Houston, TX, USA: Society of Exploration Geophysicists, Aug. 2019, pp. 107–111.

[33] N. Kilic and V. C. Gungor, "Analysis of low power wireless links in smart grid environments," *Comput. Netw.*, vol. 57, no. 5, pp. 1192–1203, Apr. 2013.
[34] J. G. Proakis and M. Salehi, *Digital Communications*, 5th ed. New York, NY, USA: McGraw-Hill, 2008.

NAVEED IQBAL received the B.S. and M.S. degrees in electrical engineering from the University of Engineering and Technology, Peshawar, Pakistan, and the Ph.D. degree from the King Fahd University of Petroleum and Minerals, Saudi Arabia. He is currently a Research Assistant Professor with the King Fahd University of Petroleum and Minerals. His research interests include adaptive algorithms, compressive sensing, heuristic algorithms, seismic signal processing, machine learning, and data acquisition networks. He has more than 30 publications in international journals/conferences and nine patents in the aforementioned areas.

SUHAIL AL-DHARRAB (Senior Member, IEEE) received the B.Sc. degree in electrical engineering from the King Fahd University of Petroleum and Minerals, Dhahran, Saudi Arabia, in 2005, and the M.A.Sc. and Ph.D. degrees in electrical and computer engineering from the University of Waterloo, Waterloo, ON, Canada, in 2009 and 2013, respectively. He is currently an Assistant Professor with the Electrical Engineering Department, King Fahd University of Petroleum and Minerals. His research interests include wireless communication systems, underwater acoustic communication, digital signal processing, and information theory.

ALI H. MUQAIBEL (Senior Member, IEEE) received the B.Sc. and M.Sc. degrees from the King Fahd University of Petroleum and Minerals (KFUPM), Dhahran, Saudi Arabia, in 1996 and 1999, respectively, and the Ph.D. degree from the Virginia Polytechnic Institute and State University (Virginia Tech), Blacksburg, in 2003. During his study at Virginia Tech, he was with the Time Domain and RF Measurements Laboratory and the Mobile and Portable Radio Research Group. He was a Visiting Associate Professor with Villanova University, Villanova, PA, USA, where he was with the Center of Advanced Communications (CAC), in 2013, and a Visiting Scholar with the Georgia Institute of Technology, in 2015. He was a Visiting Professor with the King Abdullah University for Science and Technology (KAUST), from 2018 to 2019. He is currently an Associate Professor with the Electrical Engineering Department, KFUPM. He has authored two book chapters and more than 120 articles. His current research interests include the direction of arrival estimation (DOA), through wall imaging, localization, channel characterization, and ultra-wideband (UWB) signal processing. He received many awards in the excellence in teaching, advising, and instructional technology.

WESSAM MESBAH (Senior Member, IEEE) received the B.Sc. and M.Sc. degrees (Hons.) in electrical engineering from Alexandria University, Alexandria, Egypt, in 2003 and 2000, respectively, and the Ph.D. degree from McMaster University, Hamilton, ON, Canada, in 2008. From 2009 to 2010, he was a Postdoctoral Research Fellow with Texas A&M University, Doha, Qatar. He joined the Electrical Engineering Department, King Fahd University of Petroleum and Minerals, in 2010, where he is currently an Associate Professor. His research interests include cooperative communications and relay channels, layered multimedia transmission, wireless sensor networks, multiuser MIMO/OFDM systems, cognitive radio, optimization, game theory, and smart grids.

GORDON L. STÜBER (Fellow, IEEE) received the B.A.Sc. and Ph.D. degrees in electrical engineering from the University of Waterloo, Waterloo, ON, Canada, in 1982 and 1986, respectively.

In 1986, he joined the School of Electrical and Computer Engineering, Georgia Institute of Technology, where he is currently the Joseph M. Pettit Chair Professor in Communications. He has over 300 refereed publications in journals and conferences in these areas and has graduated 32 Ph.D. students. He is the author of the textbook *Principles of Mobile Communication 4/e* (Springer International Publishing AG, 2017). His research interests include wireless communications and communication signal processing. He served as the Technical Program Chair for the 1996 IEEE Vehicular Technology Conference (VTC 1996), the Technical Program Chair for the 1998 IEEE International Conference on Communications (ICC 1998), the General Chair for the Fifth IEEE Workshop on Multimedia, Multiaccess and Teletraffic for Wireless Communications (MMT 2000), the General Chair for the 2002 IEEE Communication Theory Workshop (CTW 2002), the General Chair of the Fifth YRP International Symposium on Wireless Personal Multimedia Communications (WPMC 2002), and the General Co-Chair of the 2019 IEEE Vehicular Technology Conference (VTC 2019 Fall). He served as an elected Member-at-Large on the IEEE Communications Society Board of Governors, from 2007 to 2009. He is currently an elected member of the IEEE Vehicular Technology Society Board of Governors for the period of 2001–2021.